11th International Workshop on Ship and Marine Hydrodynamics
Hamburg, Germany, September 22-25, 2019

Scale Effect on the Hydrodynamic Performance of a Ducted Propeller under Consideration of Flow Transition and Cavitation

E. Schomburg[1,*], M. Abdel-Maksoud[2]

[1]Schiffbau-Versuchsanstalt Potsdam GmbH, Marquardter Chaussee 100, 14469 Potsdam, Germany
[2]Hamburg University of Technology, Institute for Fluid Dynamics and Ship Theory
Am Schwarzenberg-Campus 1, 21073 Hamburg, Germany

*Corresponding author, schomburg@sva-potsdam.de

ABSTRACT

The paper presents a numerical investigation of the scale / Reynolds number effects on the hydrodynamic performance of a 4-bladed ducted propeller under open water test conditions. In the numerical simulations, the influences of flow transition and cavitation are taken into account. The RANS calculations are carried out using the ANSYS-CFX solver. For turbulence modelling, the Explicit Algebraic Reynolds Stress Model (EARSM) is applied in combination with the γ-Re_θ transition model. The cavitation model employed is based on the Rayleigh-Plesset equation. In order to evaluate the various Reynolds number effects separately, different geometrical configurations are investigated. The first configuration is a 2D NACA66Amod hydrofoil. In this case, the investigation focuses on the laminar-turbulent flow-transition behaviour on the surface of the hydrofoil. In order to be able to study this behaviour on 3D geometries, a simplified blade geometry based on the hydrofoil mentioned above is developed and integrated in a neutral free-slip duct, which produces zero thrust. This configuration allows for investigating the flow transition at different regions of the rotating blade. Additionally, the flow on the Wageningen 19A duct is simulated in order to evaluate the scale effect on the hydrodynamic performance of the duct without considering scale influence induced by the propeller. In this case, the propeller flow is simulated using an actuator disc model. The final geometrical configuration is a ducted propeller that consists of a 4-bladed propeller in combination with the Wageningen 19A duct. The investigation of this configuration focuses on the change of the flow behaviour and the hydrodynamic characteristics over a wide range of Reynolds numbers. The influence of the Reynolds number on the thrust-torque ratio of the ducted propellers, particularly on the thrust breakdown behaviour at three propeller loads, is evaluated.

Keywords: Cavitation, Ducted propeller, Flow transition, RANS CFD, Reynolds number effect, Scale effect

1 INTRODUCTION

The design, calculation and testing of ducted propellers is more demanding than with conventional propellers because of the strong interactions between the duct and the propeller. A substantial body of research on ducted propeller systems in the last decades has focused on scale effect. One reason for this is the high degree of uncertainty in predicting the performance of ships fitted with ducted propellers. As a generally accepted Reynolds number correction method is not available, extrapolating the experimental and computational results from model scale to full scale remains the main source of uncertainty, and in many cases, the results of full-scale CFD computations do not correlate well with ship trial measurements. As such, the "International Towing Tank Committee" (ITTC) still recommends, contrary to free running propulsion systems, that Reynolds number corrections should not be conducted for ducted propeller systems [1] as it is argued that the thrust and torque coefficients extrapolated according to Froude's law of similarity often provide a good match between model scale and full scale. Applying Froude's method for extrapolating the model tests, which are carried out at different scales, often leads to different performance predictions in full scale. The resulting uncertainties are especially high for the case of bollard pull condition.

The SVA Potsdam has conducted model tests with ducted propulsion systems since the 1950s and has also carried out different research projects including geosim model tests and CFD-calculations to investigate possible reasons for discrepancies between the propulsion power prognosis based on the model test results and the measured values in full scale. The results show that, regardless of the Reynolds number effect, taking certain measures into consideration is important for reducing the differences between the thrust and moment coefficients for model and full scale: Model tests should be carried out with the final propeller design and the propeller pitch of the full-scale ship needs to be predicted and adapted to the full scale operation point. And if any risk regarding cavitation-induced thrust breakdown is detected, cavitation tests must be performed. Under consideration of these recommendations, the Froude-scaled bollard pull results measured during the model test will lead to a noticeable improvement in the accuracy of propulsion power prognosis. The results of the SVA Potsdam model tests and CFD studies as well as recent publications show a significant scale effect (up to 10% efficiency increase) that could not be observed in sea trials. Therefore, further research activities are required to investigate the physical phenomena associated with scale effect but also to evaluate the driving factors for not achieving the efficiency predicted by CFD investigations at full scale.

It is important to point out that in most published CFD studies on the influence of the Reynolds number on the performance of ducted propeller systems the flow was considered as fully turbulent [2], [3]. Recent publications confirm that the laminar-turbulent transition at model scale can have a significant influence on the performance of free running [4] and ducted propellers [5]. The comparison between the results of paint tests on model propellers and those of different simulations show that RANS calculations in combination with transition models are able to predict the laminar-turbulent transition with adequate accuracy [6], [7].

The paper presents a study of the Reynolds number effect on the behaviour of the flow for different simple geometrical configurations. Additionally, the flow on a 4-bladed ducted propeller is investigated with a focus on laminar-turbulent flow transition and cavitation in open water test condition.

2 APPROACH

The effect of the Reynolds number on the hydrodynamic characteristics of the components of a ducted propulsion system depends on both global and local flow conditions. In order to study the flow behaviour on each component separately, different geometrical configurations are developed, and varying aspects are focused on during the investigations. The first one is the Reynolds number effect on the hydrodynamic characteristics of a 2D hydrofoil, which is compared with those of simplified 3D blade geometry. The second aspect is the Reynolds number effect on the hydrodynamic performance of a Wageningen 19A duct. The propeller is modelled in this case as an actuator disc with predefined fixed thrust and torque coefficients. This procedure allows for avoiding a Reynolds number effect on the hydrodynamic performance of the propeller, which could influence the duct behaviour. Afterwards, the combined effect of the Reynolds

number on the performance of the duct and on the propeller is studied. In a last stage, scale effect at different Reynolds numbers on the hydrodynamic characteristics of a ducted propeller is investigated under consideration of cavitation inception and thrust breakdown.

All calculations are carried out using the ANSYS CFX solver and the Explicit Algebraic Reynolds Stress Model (EARSM) turbulence model, partly in combination with the γ-Re_θ transition model and a cavitation model based on the Rayleigh-Plesset equation. The EARSM model represents an extension of the standard two-equation model, which is derived from the Reynolds stress transport equations and gives a nonlinear relation between the Reynolds stresses and the mean strain-rate and vorticity tensors. Due to the higher order terms, many flow phenomena are included in the model without the need to solve additional transport equations. The EARSM enables an extension of turbulence models to capture secondary flows and flows with streamline curvature and system rotation [8]. By using the BSL-EARSM turbulence model, the captured expansion and vorticity of the tip vortex, which is very important for ducted propulsion systems, is increased compared to the commonly used *k-ω* SST turbulence model (Figure 1). The CFD-calculations with the γ-Re_θ transition model have higher requirements regarding the numerical mesh resolution compared to a fully turbulent calculation. The meshes of the test cases have more than 120 cells along flow direction. During grid generation, care is taken to ensure a dimensionless wall distance of $y+ < 1$ and an expansion ratio of 1.2 normal to the wall.

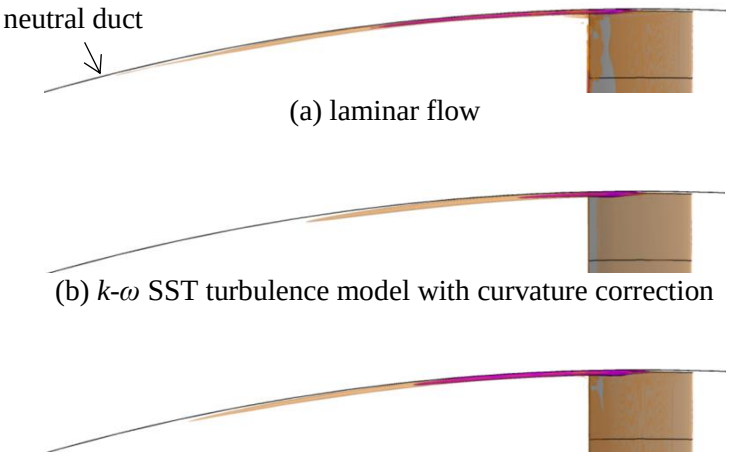

Figure 1: Constant vorticity and pressure zones computed on the 3D hydrofoil in a neutral duct, Comparison between the flow behaviour for laminar and turbulent flows calculated using two different RANS turbulence models, (beige: vorticity $\lambda \approx 1850$ 1/s, violet: pressure $C_P = -0.25$)

3 GEOMETRIES

The NACA66Amod hydrofoil is considered in the study because such a foil section is typical for marine propellers. The NACA66Amod hydrofoil investigated has a camber (*f*) of 2.0% and a thickness (*t*) of 3.5% (Figure 2). For the 3D test case, the hydrofoil is extruded to form a propeller blade. The blade is integrated in a neutral duct and rotates around an axis parallel to the inflow. The angle of attack is calculated in relation to the combined advanced and circumferential speed and is fixed ($\alpha = 1°$) for every blade section. The resulting pitch ratio (*P*/*D*) is approximately 1.15, the radius of the blade (*R*) is 1.0 m, the chord length of the hydrofoil (*c*) is 0.05 m, the gap size (*s*) is 1.0 mm and the number of blades (*z*) is 4. To investigate the flow transition effect at different positions, the blade is divided into different parts (Figure 3).

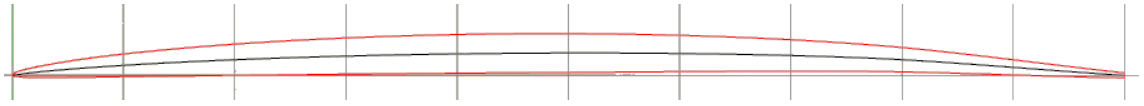

Figure 2: Test case hydrofoil, NACA 66Amod, $f = 2.0\%$, $t = 3.5\%$

For the investigation of the Reynolds number effect on the hydrodynamic performance of a duct, the well-known Wageningen 19A is considered. This duct is one of the most frequently built propeller ducts. The geometry was developed in the 1950s within a propeller nozzle test series [9]. An actuator disc model is applied to take the propeller influence on the duct flow into account and at the same time to keep defined forces induced by the propeller. The actuator disc is positioned at 50% of the duct length. Only a duct segment is modelled as the problem is considered to be axisymmetric (Figure 4).

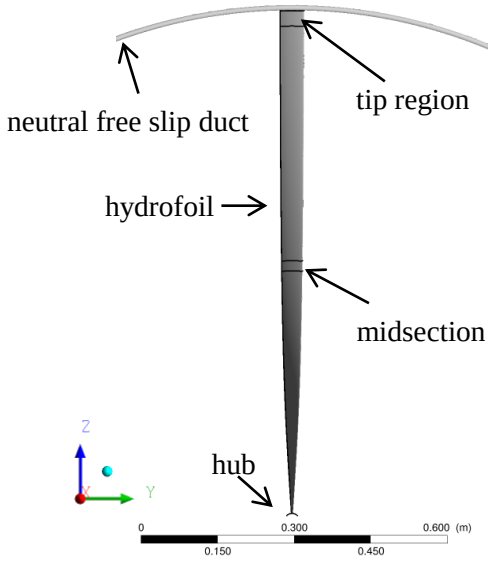

Figure 3: 3D rotating hydrofoil test case

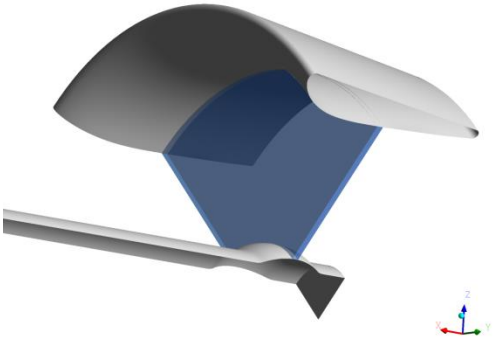

Figure 4: Wag. 19A duct segment with actuator disc

A 4-bladed propeller in combination with the Wageningen 19A duct is considered in the propeller test case. The propeller has a pitch ratio of P/D = 1.2 and blade area ratio of A_E/A_0 = 0.675. The gap between blade tip and the inner wall of the duct (s) is $0.0075 \cdot D$.

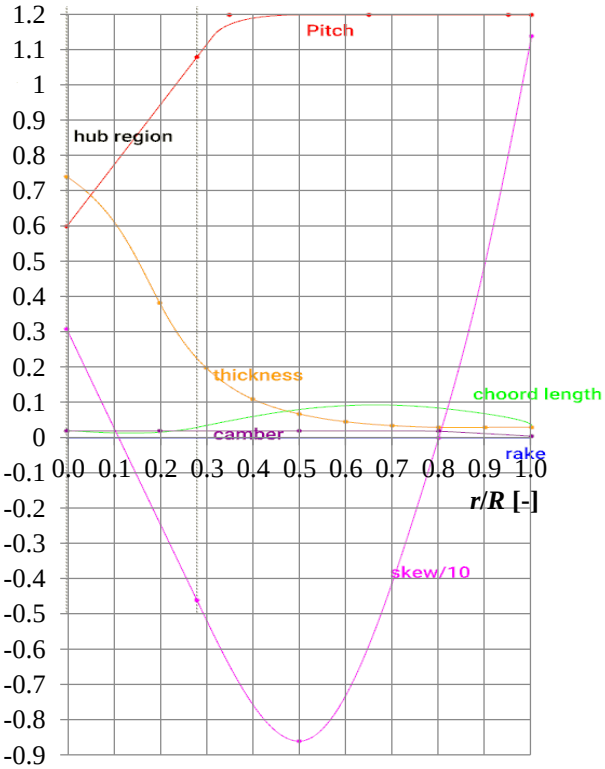

(a) Propeller definition curves

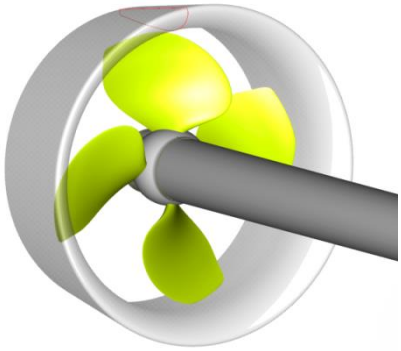

(b) Propeller system geometry

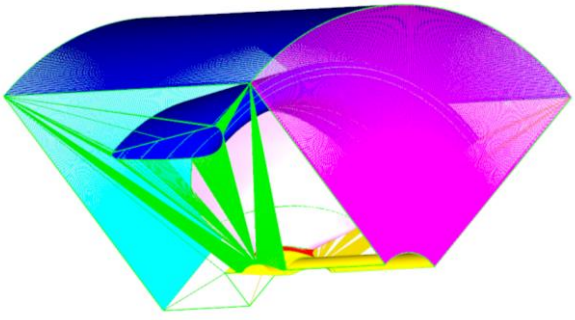

(c) Inner rotating domain for CFD calculation

Figure 5: Propeller geometry and rotating CFD domain

The propeller geometry is considered as a basis for a geometrical parameter variation study. Therefore, it has an almost constant pitch and almost constant camber. Additionally, the chord length of the blade is kept short at the hub radius to allow for a gap-free pitch adjustment in upcoming model tests. Above radius $r/R > 0.5$, the NACA66Amod hydrofoil is used. To reduce the risk of cavitation and flow separation, the pitch below radius $r/R < 0.5$ is reduced and the hydrofoil changes continuously to a NACA 4-digit profile at the hub radius. The geometry of the propeller system is shown in Figure 5 (a) and (b). As the propeller flow simulation is carried out under parallel inflow conditions, one propeller blade is considered in the numerical simulations while the influence of the other blades is taken into account by applying the periodical boundary condition at the sides of the calculation domains (Figure 5 (c)).

4 NUMERICAL INVESTIGATIONS

4.1 2D NACA66Amod hydrofoil test case

The flow simulations for the 2D test case are carried out with and without applying the γ-Re_θ transition model in order to study the effect of the flow transition behaviour at different angles of attack and different Reynolds numbers (Eq. 1). The evaluation is based on the lift coefficient (Eq. 2) and the drag coefficient (Eq. 3) as well as on the friction coefficient (Eq. 4) and the lift-to-drag ratio (Eq. 5). Additionally, the relative laminar blade surface area to the total wetted area is evaluated. The Reynolds number effect on hydrodynamic coefficients for two typical angles of attack of a working propeller are shown in Figure 6.

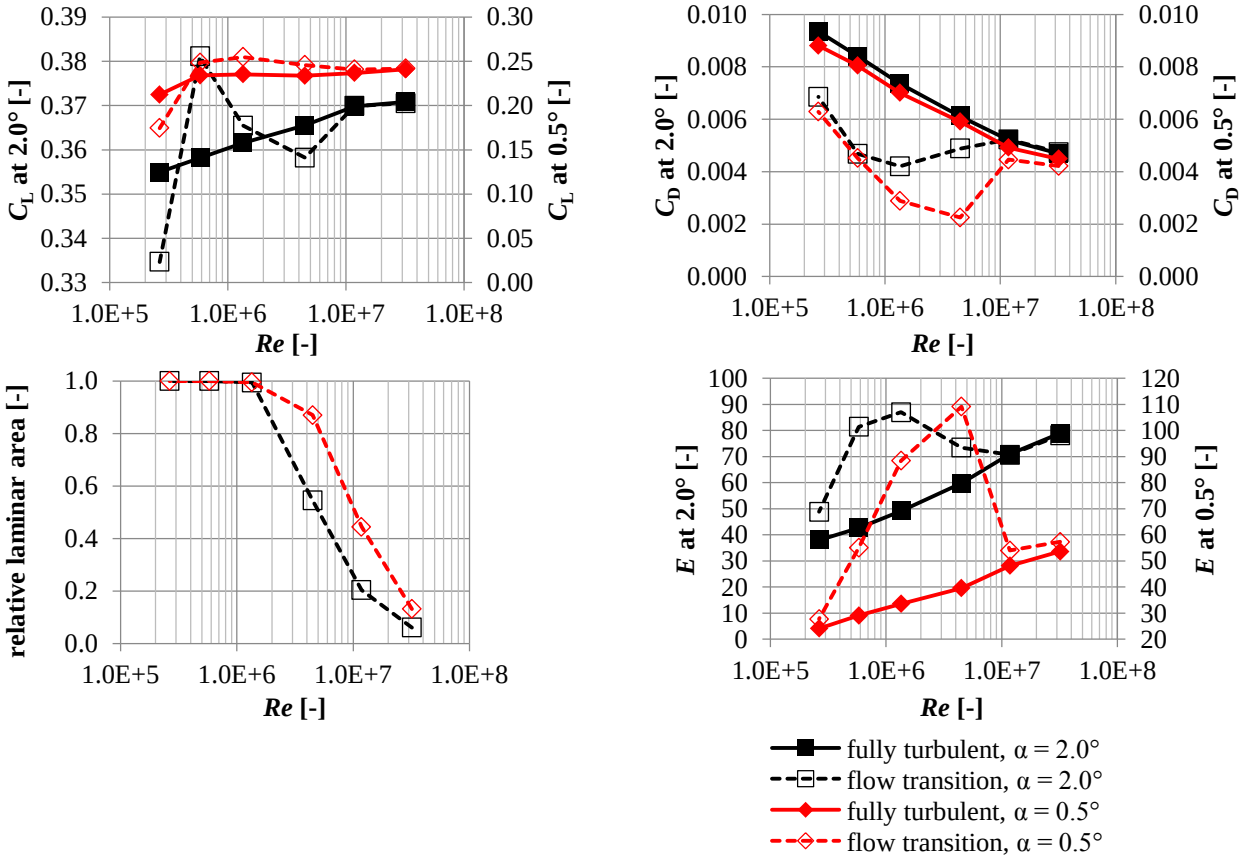

Figure 6: Reynolds number effect on characteristic values of a 2D NACA 66Amod hydrofoil

$$Re = \frac{v_\infty \cdot l}{\vartheta} \tag{1}$$

$$C_L = \frac{F_z}{\frac{\rho}{2} \cdot v_\infty^2 \cdot A} \tag{2}$$

$$C_{\mathrm{D}} = \frac{F_{\mathrm{x}}}{\frac{\rho}{2} \cdot v_{\infty}^{2} \cdot A} \tag{3}$$

$$C_{\mathrm{f}} = \frac{F_{\mathrm{fx}}}{\frac{\rho}{2} \cdot v_{\infty}^{2} \cdot A} \tag{4}$$

$$E = \frac{C_{\mathrm{L}}}{C_{\mathrm{D}}} \tag{5}$$

The friction force could be split into suction-side friction and pressure-side friction (Figure 7). Compared with the pressure side, it can be seen that flow transition occurs at the suction side at lower Reynolds numbers and with a more or less sudden flow transition. The flow transition on the pressure side occurs more gradually. As it can be seen from the results of the 2D test case, the location of the laminar-turbulent flow transition depends on the Reynolds number but also on the angle of attack.

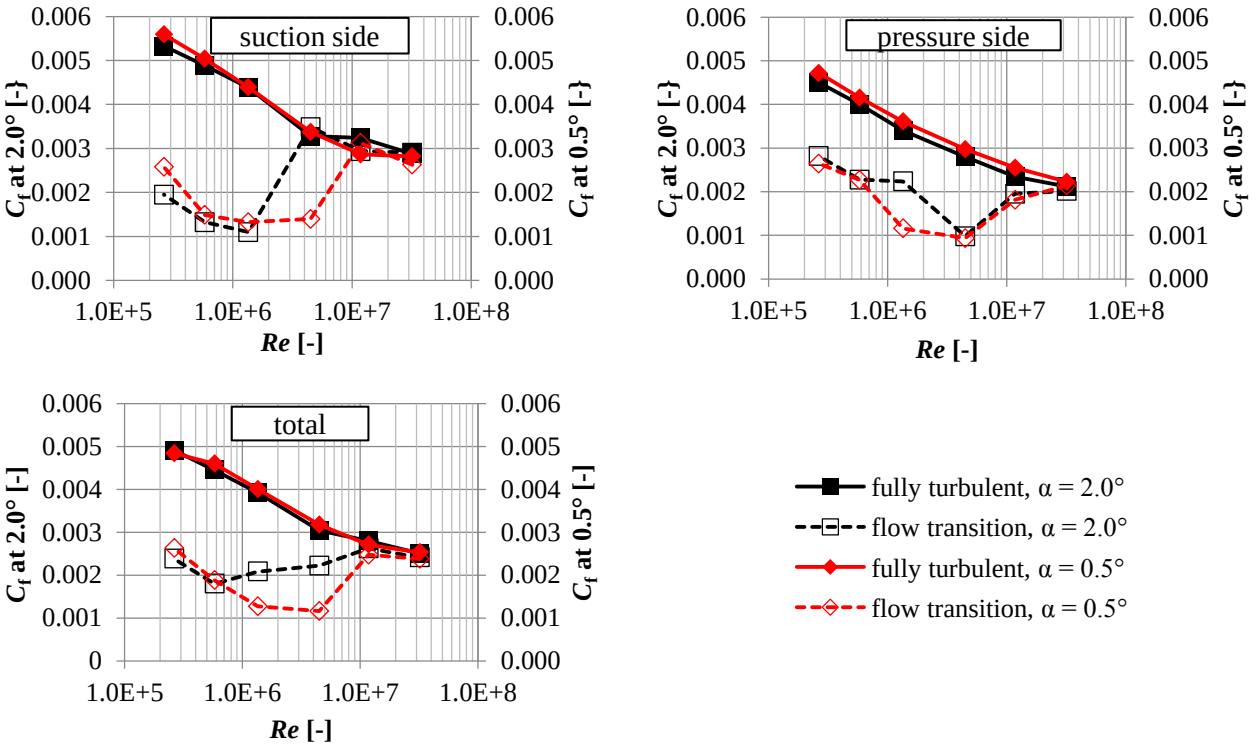

Figure 7: Reynolds number effect on the friction coefficient for a 2D NACA 66Amod hydrofoil

The obtained simulation results based on fully turbulent flow computations show that increasing the Reynolds number leads to a steady increase in the lift and decrease in the drag; the trend of the lift and drag coefficients under consideration of the flow transition is more complex. The flow characteristic is strongly dependent on the area extension of the laminar boundary layer and the boundary layer thickness. Below $Re < 5\times10^{5}$, the boundary layer leads to a laminar flow separation zone on the trailing edge area of the suction side and therefore a significant impact to the lift and drag can be observed. Up to $Re < 2\times10^{6}$, this separation zone could still be present but its impact on the lift and drag decreases. The highest lift to drag ratio is achieved at a condition of maximised laminar boundary layer extension without any flow separation. For the investigated geometry, this condition takes place between $1\times10^{6} < Re < 5\times10^{6}$ depending on the angle of attack (Figure 8). For $Re > 5\times10^{6}$, the boundary layer starts to be more turbulent and the efficiency of the hydrofoil strongly decreases compared to previous condition, but the lift drag ratio will rise with a further increase in the Reynolds number. The displacement effect of the hydrofoil stabilises the boundary layer due to the negative pressure gradient, which leads to a longer laminar zone compared to the flat plate

friction presented in [10] (Figure 9). A correction based only on the flat plate boundary layer theory seems to be inadequate for considering the Reynolds number effect at 2D flows.

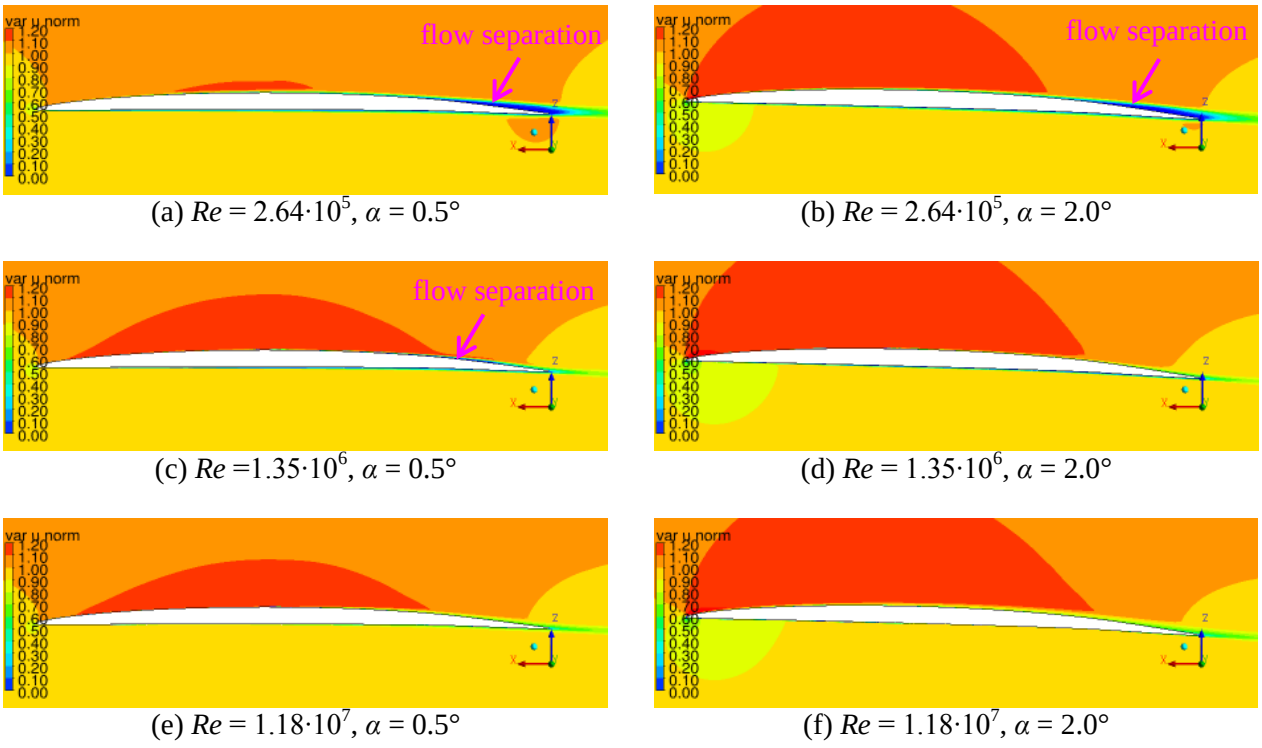

(a) $Re = 2.64 \cdot 10^5$, $\alpha = 0.5°$ (b) $Re = 2.64 \cdot 10^5$, $\alpha = 2.0°$

(c) $Re = 1.35 \cdot 10^6$, $\alpha = 0.5°$ (d) $Re = 1.35 \cdot 10^6$, $\alpha = 2.0°$

(e) $Re = 1.18 \cdot 10^7$, $\alpha = 0.5°$ (f) $Re = 1.18 \cdot 10^7$, $\alpha = 2.0°$

Figure 8: Normalised velocity field for different Reynolds numbers at $\alpha = 0.5°$ and $\alpha = 2.0°$

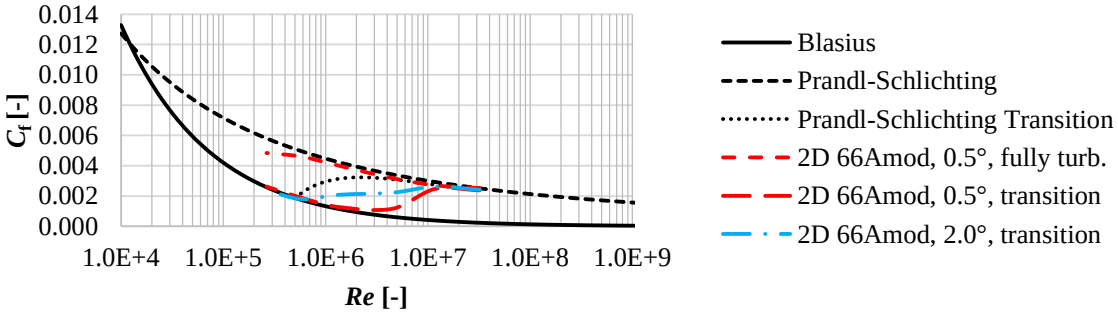

Figure 9: Flat plate friction compared with 2D friction of a NACA66Amod hydrofoil

4.2 3D NACA66Amod rotating hydrofoil in a neutral free slip duct

The hydrodynamic characteristics of propellers are pressure dominated. Moreover, the blade rotation induces centrifugal and Coriolis forces to the flow that have an additional impact. In this section, the flow on a rotating 3D hydrofoil in a neutral duct is investigated.

The computations for investigating the influence of the flow transition in the 3D test case are carried out at an advanced coefficient of $J = 1.1$ to achieve the desired blade section angel of attack of $\alpha \approx 1°$. The thrust coefficient in x-direction (Eq. 7) and the torque coefficient around the x-axes (Eq. 8) are evaluated at two radial blade zones at the tip ($0.97 \leq r/R \leq 1.0$) and at midsection ($0.49 \leq r/R \leq 0.51$) using the local Reynolds number (Eq. 6, Eq. 9).

$$v_{\mathrm{loc}} = \sqrt{v_\infty^2 + (\pi \cdot r \cdot n)^2} \qquad (6)$$

$$C_{Fx} = \frac{F_x}{\frac{\rho}{2} \cdot v_{\text{loc}}^2 \cdot A} \cdot 10^3 \qquad (7)$$

$$C_{Mx} = \frac{M_x}{\frac{\rho}{2} \cdot v_{\text{loc}}^2 \cdot A \cdot r} \cdot 10^3 \qquad (8)$$

$$Re = \frac{v_{\text{loc}} \cdot c}{\vartheta} \qquad (9)$$

The calculation results show that the Reynolds number effect on the blade characteristics are dominated by the Reynolds number effect on the pressure force (Figure 10, Figure 11). For the calculations without transition model, the thrust coefficient increases with increasing Reynolds number. The torque coefficient at the midsection is almost independent of the Reynolds number and is decreasing with increasing Reynolds number at the tip region. In the calculations with transition model, the thrust and torque coefficient reach their maximum values around $Re \approx 1.5 \times 10^6$. Below this Reynolds number, a flow separation zone at the trailing edge of the suction side leads to pressure losses. Above this Reynolds number, the partially turbulent boundary layer also leads to a reduced pressure force on the hydrofoil, which slightly reduces with further increasing Reynolds number.

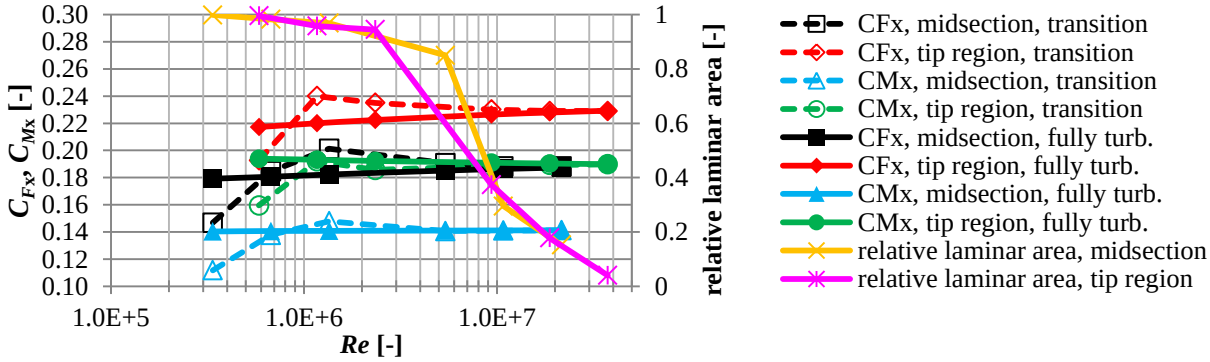

Figure 10: Influence of the Reynolds number on the thrust and torque coefficients of a rotating 3D hydrofoil test case

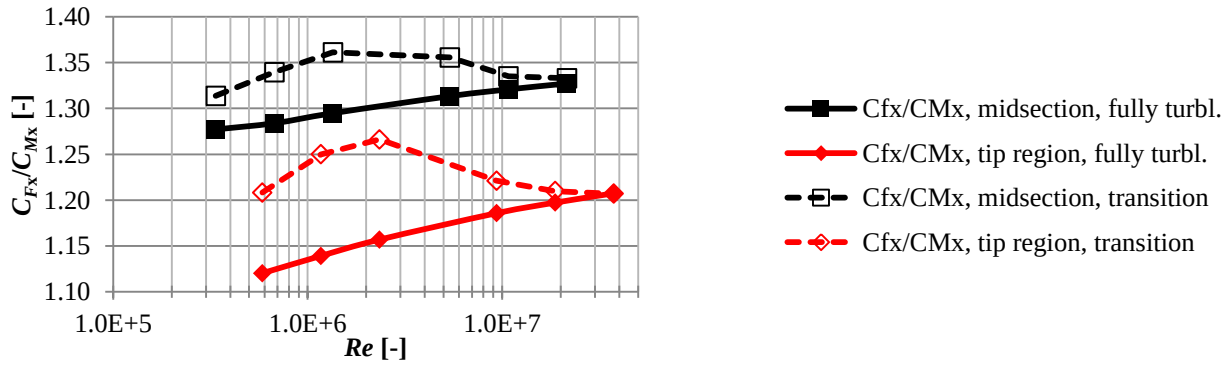

Figure 11: Influence of the Reynolds number on the thrust-torque ratio for a rotating 3D hydrofoil test case

4.3 Comparison of the 2D and 3D test case

The results of both test cases show a similar behaviour and confirm the significant influence of the boundary layer flow transition on the Reynolds number effect. However, for the 3D case, the strong friction influence that could be evaluated at the 2D test case is mostly negligible compared to the pressure-dominated effect which can be observed in the 3D test case. Figure 12 shows the ratio of the laminar flow area to the total wetted area as a function of Reynolds number for different angles of attack of the 2D hydrofoil and different positions of the 3D blade. The maximum lift-to-drag or thrust-to-torque ratio is reached for both

cases at a *Re* between 1×10^6 and 5×10^6, which is in line with the flow transition behaviour of the boundary layer. That leads to the assumption that a modern hydraulically smooth blade surface of a model propeller tested above $Re > 1.5\times10^6$ would not have an improved efficiency in full scale.

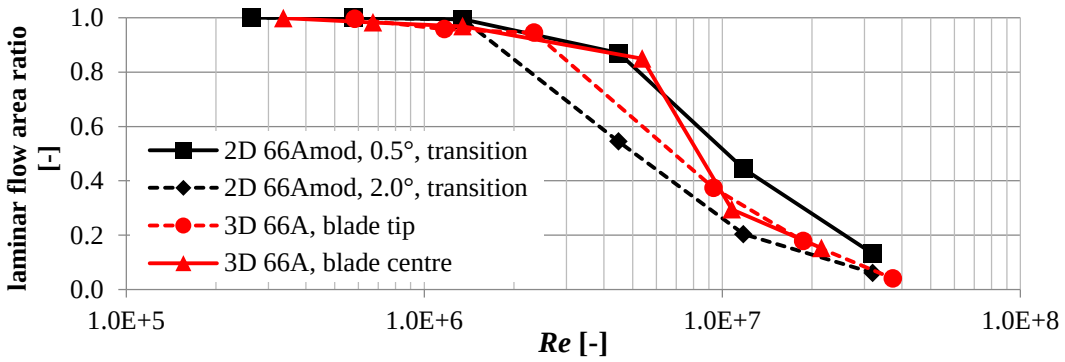

Figure 12: Relative laminar area for the 2D and 3D test cases

4.4 Reynolds number effect for a Wageningen 19A duct

For investigating the Reynolds number effect on the hydrodynamic performance of the duct, the computations are conducted for the Wageningen 19A duct with an actuator disc. The actuator disc is used to yield constant induced forces by the propeller at all scales. The considered thrust force and torque are obtained from an open water test diagram of a ducted propeller (19A Duct, P/D = 1.2, A_E/A_0 = 0.625). The force and the torque distributions are considered to be constant over circumferential direction. The influence of the gap between the inner wall of the duct and outer diameter of the actuator disc is investigated by conducting the RANS simulations with and without gap. The duct Reynolds number is defined according to Eq. 12. The influence of the rotational speed of the propeller blade is taken into account as the duct flow is strongly influenced by the propeller flow. For this reason, a thrust-independent inflow velocity is defined and used instead of the de facto inflow velocity. The thrust-independent velocity is calculated based on the $P_{0.7}/D$ ratio of the propeller, which is very close to the thrust advanced coefficient J value for zero propeller thrust (Eq. 10). In this case, the pitch-to-diameter ratio ($P_{0.7}/D$) value of the propeller simulated can be used to define a duct inflow velocity independent of an actual propeller operating point (Eq. 11). This velocity is used to calculate the duct friction coefficient (Eq. 13).

To correctly interpret the friction coefficient, some aspects should be considered. While the flow velocity on the outer duct side rises with increasing J, in the same manner the flow velocity on the inner duct side increases only slightly. The higher flow velocity inside and outside the duct leads to increased friction forces. As the flow velocities on the inner and outer duct surface are different, the friction coefficient is partially shown for both sides.

$$J = \frac{v}{n \cdot D} \tag{10}$$

$$v_{\mathrm{D}} = P_{0.7}/D \cdot n \cdot D \tag{11}$$

$$Re_{\mathrm{D}} = \frac{v_{\mathrm{D}} \cdot l_{\mathrm{D}}}{\vartheta} \tag{12}$$

$$C_{\mathrm{fD}} = \frac{F_{\mathrm{f}}}{\frac{\rho}{2} \cdot v_{\mathrm{D}}^2 \cdot A} \tag{13}$$

$$K_{T\mathrm{D}} = \frac{T_{\mathrm{D}}}{\rho \cdot n^2 \cdot D^4} \tag{14}$$

The results of the fully turbulent flow calculations show for the duct case and for the 2D and 3D lifting bodies similar hydrodynamic behaviours. The increase of the Reynolds number leads to a decreasing friction force coefficient and increasing duct thrust coefficient K_{TD} (Eq. 14), as shown in section 4.1 (Figure 13) for fully turbulent calculations. Under consideration of flow transition, the calculated friction coefficients of the duct surface without a gap between actuator disc and duct do not show common tendencies (Figure 14). This is a result of different Reynolds number separation behaviours. Flow separation takes place on the inner surface of the duct behind the leading edge at small J and in the diffusor region. On the outer surface, the flow separation occurs at medium and high advanced coefficients influence the flow. The flow separation dominates the duct friction at operating points of $Re < 0.6\times10^6$. Furthermore, the duct forces at smaller advanced coefficients are mainly dominated by the pressure forces, so the friction has a limited contribution to the total force.

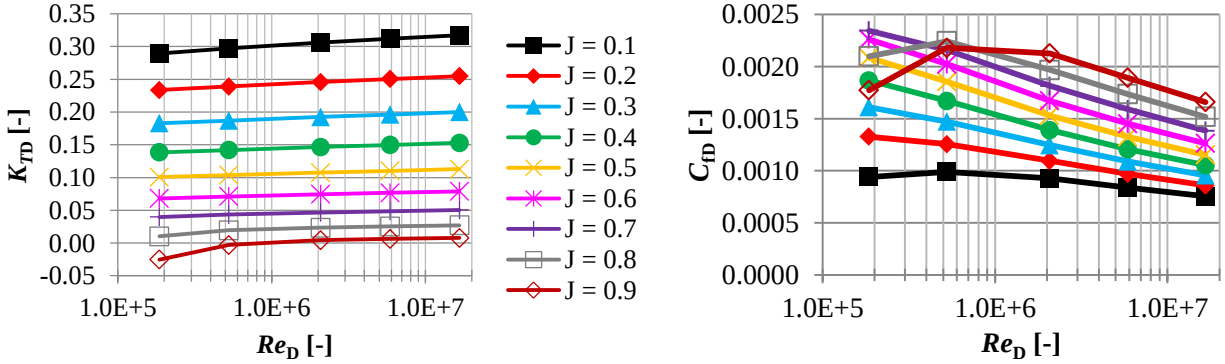

Figure 13: Reynolds number effect with fully turbulent calculation, 19A duct and actuator disc without gap

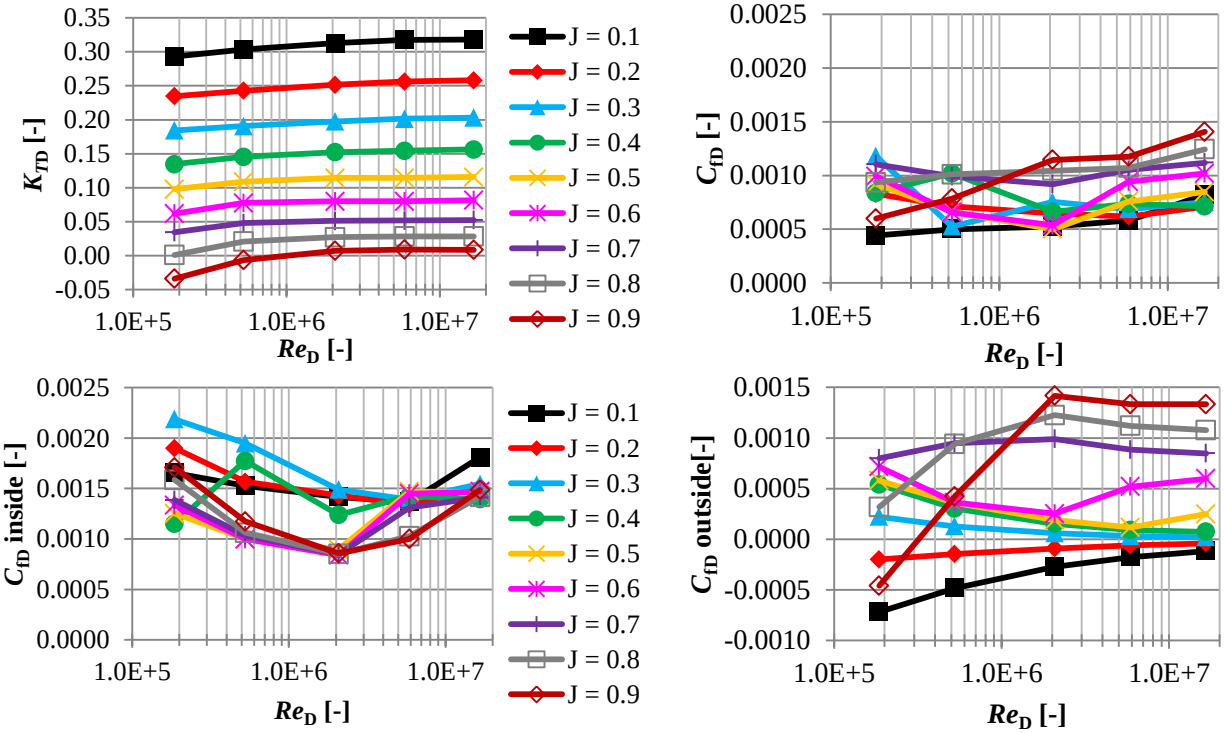

Figure 14: Reynolds number effect with flow transition, 19A duct and actuator disc without gap

Introducing a gap of $s = 0.005{\cdot}D$ between the inner wall of the duct and actuator disc leads to a different Reynolds number effect. In general, the duct forces are reduced and due to the interaction of the duct boundary layer with the gap flow, the actuator disc generates a Reynolds number-dependent vortex in the gap region and a fully turbulent flow behind the actuator disc, which avoids diffusor flow separation in the test cases investigated. The strength of the vortex is highly influenced by the thickness of the boundary layer and by the duct thrust. High vortex strength in the gap region leads to a more disturbed flow behind the

actuator disc and to a reduction in the duct thrust in combination with strongly reduced friction forces (Figure 15).

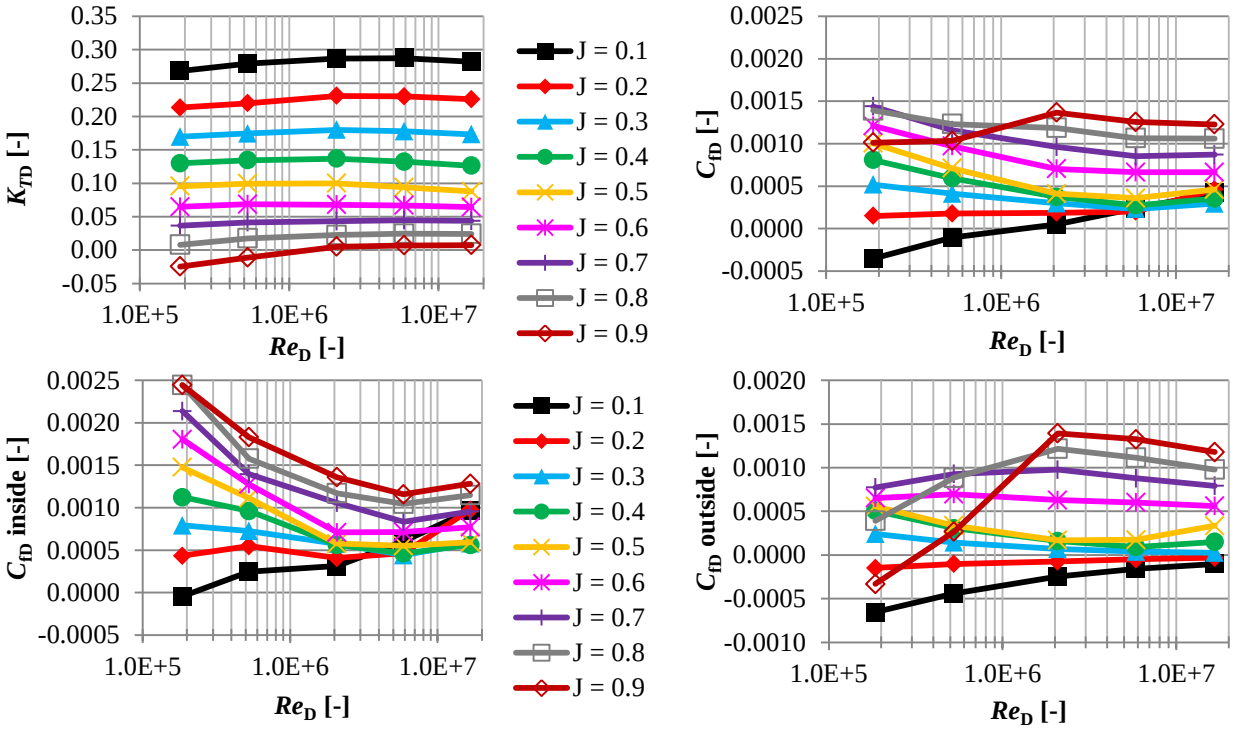

Figure 15: Reynolds number effect with flow transition, 19A duct and actuator disc with gap

At Re of > 5×10^6, a reduction of the thrust duct takes place due to the influence of the boundary layer on the gap vortex (Figure 16). For Re < 1×10^6, the laminar flow separates on the inner duct surface. The consequences are a gap vortex with a relative high strength and reduced diffusor performance, i. e. a reduced duct thrust. With increasing Reynolds number (1×10^6 < Re < 5×10^6), the laminar flow separation fades and the laminar boundary layer dominates. A minimum thickness of the boundary layer leads to a reduced tip vortex strength and so to a maximised duct thrust. At $Re \geq 5\times10^6$, the boundary layer is mostly turbulent and therefore its thickness increases compared to the laminar one.

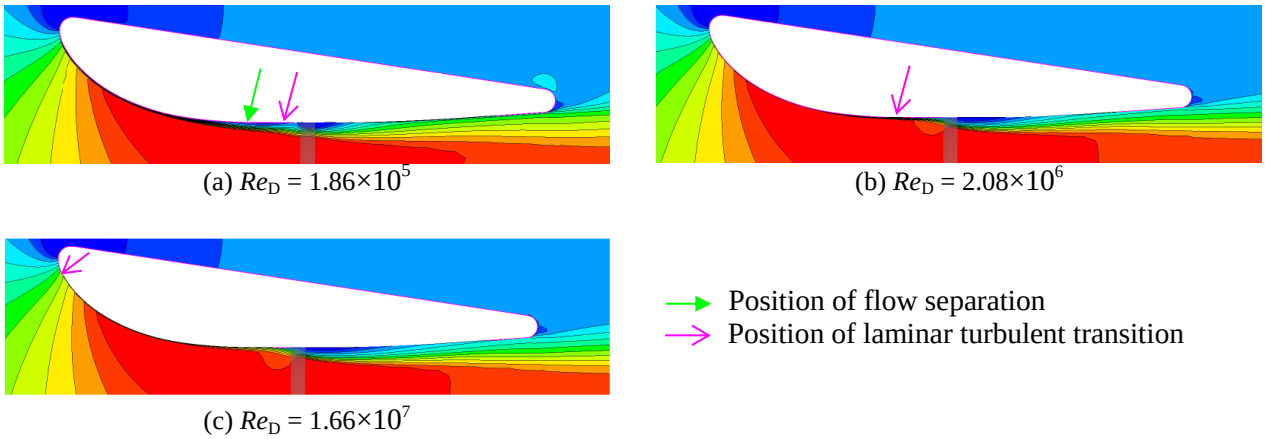

(a) $Re_D = 1.86\times10^5$ (b) $Re_D = 2.08\times10^6$

(c) $Re_D = 1.66\times10^7$

Figure 16: Flow around 19A duct, actuator disc with gap, J = 0.1

The results show that the Reynolds number effect on the duct force are influenced by a combination of the Reynolds number-dependent friction, the boundary layer thickness effect on the duct pressure and the strength of the tip vortex. The last one also depends on the wall roughness of the duct, possible flow separation on the inner duct surface as well as on geometrical characteristics such as pitch ratio, chord length of tip section and gap size.

4.5 Reynolds number effect on 4-bladed propeller with a Wageningen 19A duct

The open water propeller test case combines the Reynolds number effect on a 3D foil and on the duct geometry. In addition to Reynolds number effect, the cavitation-induced thrust breakdown is considered.

4.5.1 CFD boundary conditions

The numerical calculation domain was divided in an outer fixed domain and an inner rotating domain (Figure 5 (c)). A free slip boundary condition is applied on the propeller shaft surface to minimise the shaft boundary layer thickness. The calculations are carried out for one blade using the steady "Frozen Rotor" assumption. The previously mentioned flow transition model and cavitation model are applied in the computations. The computations are carried out for three operating points at five different scales and various cavitation numbers. It is assumed that the full-scale propeller has a diameter of D = 4.0 m with a rotational speed of n = 160 rpm. A mesh study was conducted. The resolution of the unstructured meshes that were used varied between 5.1 and 7.6 million nodes depending on the propulsion unit scale. The number of cells in flow direction is kept at more than 80. The average value of the dimensionless wall distance of the first cell is $y+ < 1$ and an expansion ratio of 1.2 normal to the wall is applied. The diffusor region was refined to have a sufficiently resolved tip vortex.

4.5.2 Reynolds number effect without cavitation

In a first step, the Reynolds number effect on a cavitation-free condition is investigated. The coefficients of the total thrust (Eq. 16), propeller thrust (Eq. 15), duct thrust (Eq. 14) and propeller torque (Eq. 17) are shown in Figure 17 and Figure 18. The results show that the total thrust slightly increases up to a Reynolds number of $1\times10^6 < Re < 5\times10^6$. At Reynolds numbers above $Re > 5\times10^6$, the total thrust decreases because of the laminar turbulent flow transition at the duct and at the propeller. With further increasing Reynolds number, the total thrust increases slightly. The Reynolds number effect on the propeller torque cannot be described in a general manner due to the coupling between the propeller thrust and the duct thrust as well as the propeller torque. Therefore, it is more useful to compare the thrust-torque ratio (Figure 19). The $K_{TP}/10K_Q$ ratio shows a minimum ratio below $Re < 1\times10^6$. The maximum ratio is reached between $1\times10^6 < Re < 5\times10^6$.

$$K_{TP} = \frac{T_P}{\rho \cdot n^2 \cdot D^4} \tag{15}$$

$$K_{TT} = \frac{T_T}{\rho \cdot n^2 \cdot D^4} \tag{16}$$

$$10K_Q = \frac{Q}{\rho \cdot n^2 \cdot D^5} \cdot 10 \tag{17}$$

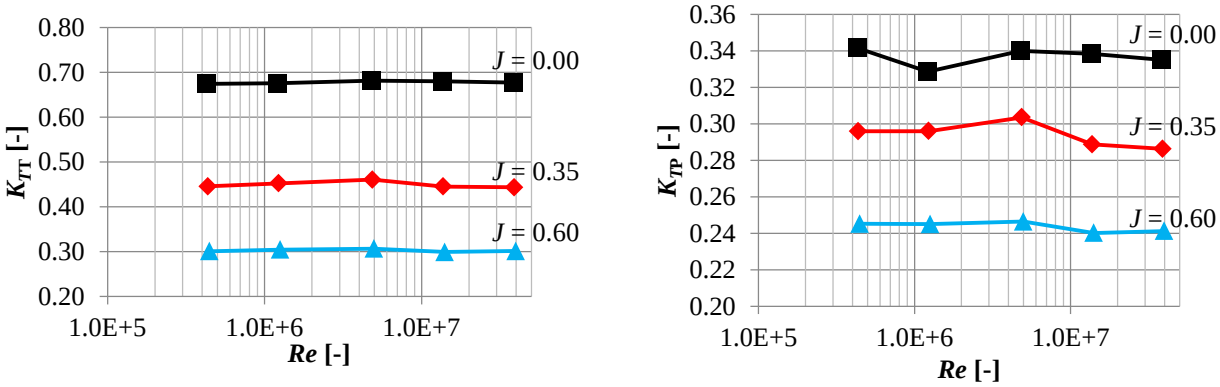

Figure 17: Reynolds number effect of the cavitation-free total ducted propeller thrust and propeller thrust coefficients

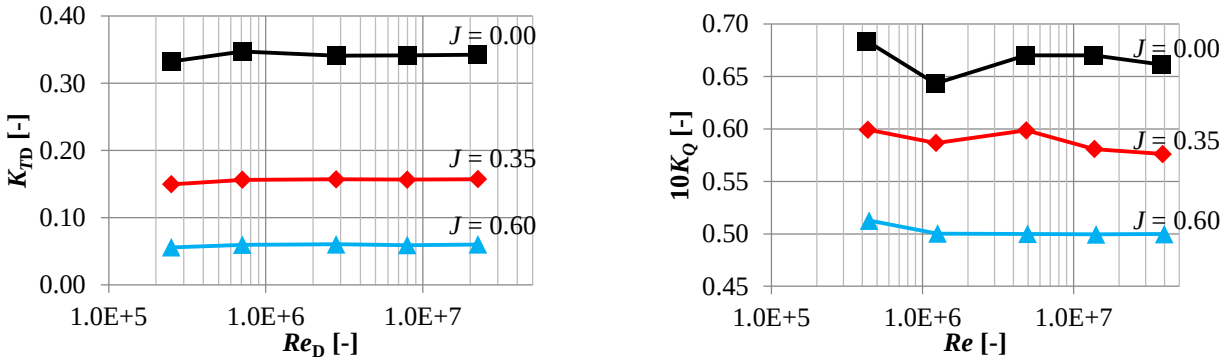

Figure 18: Reynolds number effect of the cavitation-free duct trust and propeller torque coefficients

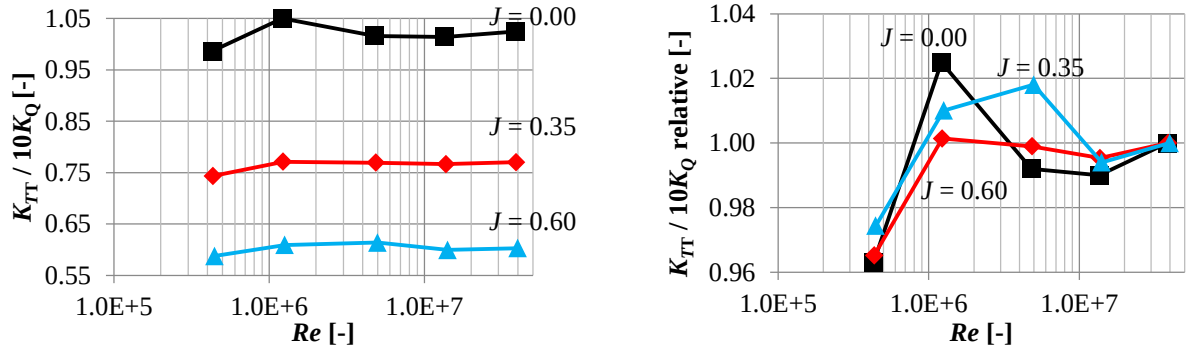

Figure 19: Reynolds number effect of the cavitation-free ducted propeller thrust-torque ratio

4.5.3 Reynolds number effect with cavitation

The Reynolds number has a considerable effect on cavitation and therefore on the cavitation-induced thrust breakdown. The definition of cavitation number applied σ_n is given in (Eq. 18), where p_{atmo}: atmospheric pressure, g: gravitational constant, h: water depth and p_v: vapor pressure. In Figure 20 (left) to 22 (left), the general influence of the Reynolds number and cavitation number is shown. In Figure 20 (right) to 22 (right), the cavitation number influence for different Reynolds numbers is shown for three operating points relative to the cavitation free condition. At bollard pull condition $J = 0$, the Reynolds number effect of the thrust-torque ratio over σ_n is non-uniform. For $Re > 1\times10^6$, an increased thrust-torque ratio at $\sigma_n \approx 4$ takes place before the thrust breakdown. The thrust breakdown appears abruptly at the same cavitation number for all Reynolds numbers at this operating point (Figure 20). At lower propeller loading conditions (Figure 21 and Figure 22), a significant Reynolds number influence on the thrust breakdown can be observed. With increasing Reynolds number, the thrust loss gradient increases. This leads to an earlier thrust breakdown.

$$\sigma_n = \frac{p_{atmo} + \rho \cdot g \cdot h - p_v}{\frac{\rho}{2} \cdot (n \cdot D)^2} \tag{18}$$

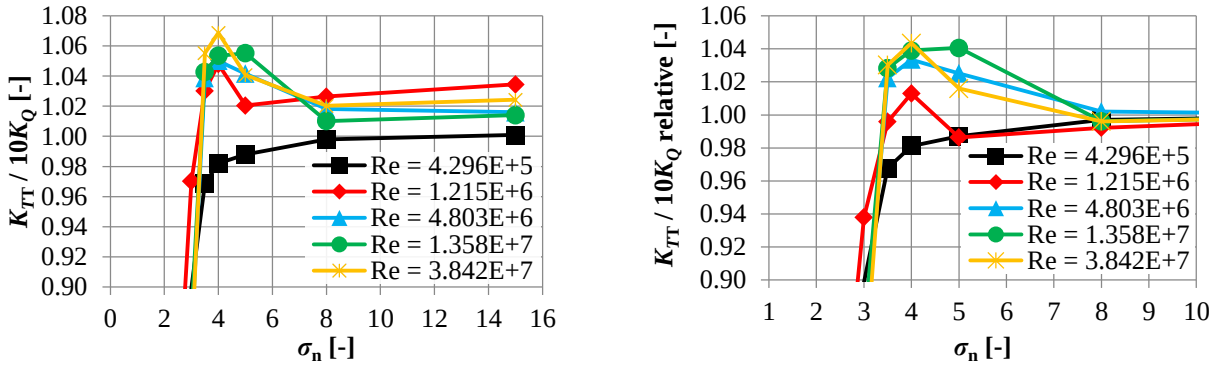

Figure 20: Reynolds number effect on a cavitating ducted propeller, J = 0.0

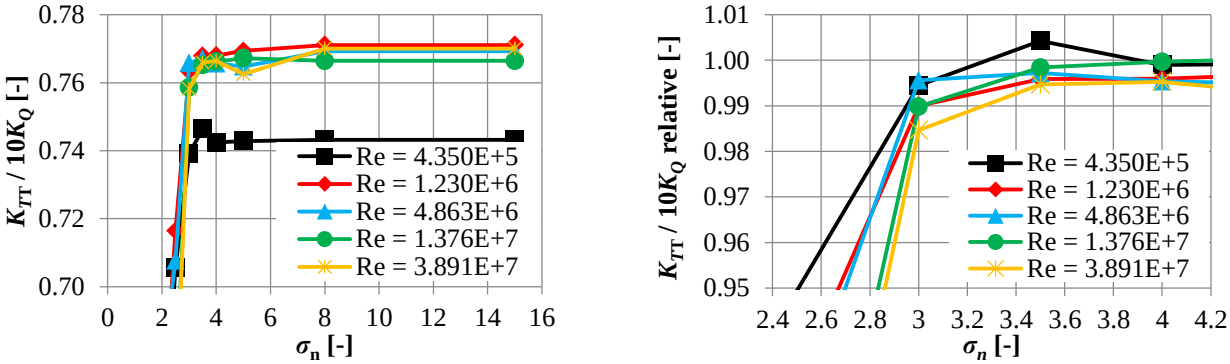

Figure 21: Reynolds number effect on a cavitating ducted propeller, J = 0.35

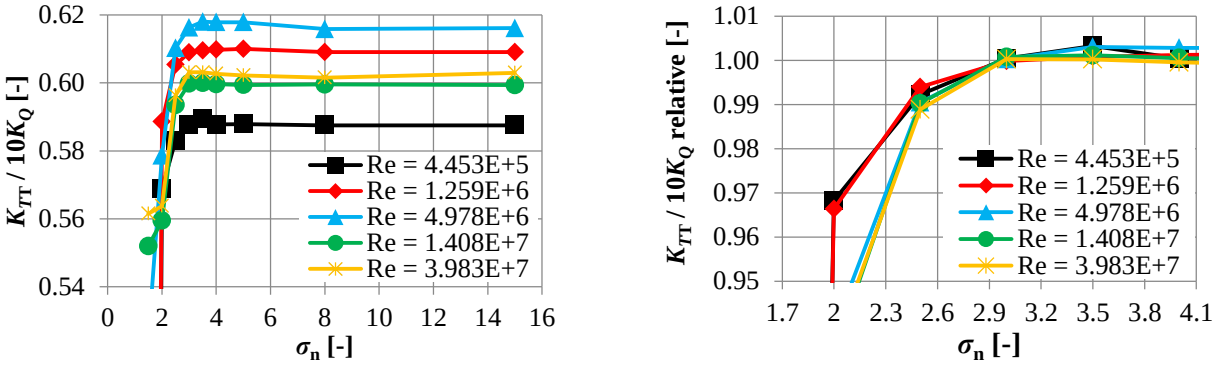

Figure 22: Reynolds number effect on a cavitating ducted propeller, J = 0.60

5 CONCLUSION

According to the results of the numerical investigations, it can be concluded that the boundary layer characteristics and particularly the laminar-turbulent flow transition have a dominating influence on the Reynolds number effect.

Compared to the (1D) flat plate, the flow transition on 2D and 3D lifting bodies occurs at significantly higher Reynolds numbers. The calculations show that friction force can have a considerable influence on the pressure force. A reduced friction force leads to a higher pressure gradient.

For $Re < 1\times10^6$, significant flow separation could occur at the 66Amod hydrofoil investigated, which has a significant influence on the lift-drag ratio for the 2D case or thrust-torque ratio for propellers. Under consideration of the flow transition, the highest efficiency is reached with a mainly laminar boundary layer between $1\times10^6 < Re < 5\times10^6$ depending on the operating point. The efficiency with fully turbulent boundary layer rises with increasing the Reynolds number but the increase is less compared to a full laminar flow

condition without flow separation. Additionally, the results show that the thrust breakdown could be dependent on the Reynolds number and therefore could occur at a higher cavitation number at the full-scale ship.

Because there is no variation of the geometrical parameter in the presented study, it is important to evaluate the validity of the above-mentioned findings for different ducted propellers with different P/D ratio, A_E/A_0 ratio, tip loading conditions and different gap sizes.

A correction of the scale effect based only on the flat plate boundary layer theory seems to be inadequate for a Reynolds number correction for ducted propellers. The quantification of the influence of the friction forces on the pressure forces on the propeller and on the duct needs an advanced extrapolation approach that is able take into account the properties of the flow at the model-scale and full-scale Reynolds numbers. According to the current results, the assumption that a ducted propeller model tested above $Re > 1.5\times10^6$ will have a significantly improved efficiency in full scale is unfortunately not appropriate.

ACKNOWLEDGEMENTS

The results presented in this paper are part of a current research project “ReProDuct”, which is founded by the German Federal Ministry for Economic Affairs and Energy within the research program “INNO-KOM-OST”. The calculations are also supported by ANSYS Inc. by providing the employed research licenses. The authors would like to express their gratitude for this valuable support.

REFERENCES

[1] ITTC - Recommended Procedures and Guidelines, *7.5-02-03-01.1 Propulsion/Bollard Pull Test*, ITTC 2011 Revision 04.

[2] M. Abdel-Maksoud and H.-J. Heinke, "Scale Effects on Ducted Propellers," in *24th Symposium on Naval Hydrodynamics*, Fukuoka, Japan, 2002.

[3] A. Bhattacharyya, V. Krasilnikov and S. Steen, "Scale Effects on a 4-Bladed Propeller Operating in Ducts of Different Design in Open Water," in *4th International Symposium on Marine Propulsors*, Austin, Texas, 2015.

[4] e. a. Pérez-Sobrino, "A New Performance Prediction Procedure for Propellers with Unconventional Tip Shape," in *12th International Conference on Hydrodynamics*, Delft, 2016.

[5] A. Bhattacharyya, J. C. Neitzel, S. Steen, M. Abdel-Maksoud and V. Krasilnikov, "Influence of Flow Transition on Open and Ducted Propeller Characteristics," *Fourth International Symposium on Marine Propulsors, smp'15,* Austin, Texas, 2015.

[6] A. Bhattacharyya, V. Krasilnikov and S. Steen, "Scale effects on open water characteristics of a controllable pitch propeller working within different duct designs," *Ocean Engineering 112,* pp. 226-242, 2016.

[7] N. Hasuike, M. Okazaki and A. Okazaki, "Flow characteristics around marine propellers in self propulsion condition," *19th Numerical Towing Tank Symposium (NuTTS 2016)* , St. Pierre d'Oleron, France, 2016.

[8] "ANSYS Users Guide," [Online]. Available: https://ansyshelp.ansys.com/account/secured?returnurl=/Views/Secured/corp/v191/cfx_thry/thry_turb_earsm.html. [Accessed 04 06 2019].

[9] J. van Manen, "Open-water test series with propeller nozzles," *International Shipbuilding Progress, vol 1,* 1954.

[10] H. Schlichting and K. Gersten, *Grenzschicht-Theorie*, Springer, 2006.